Vibrational polarization beats in femtosecond coherent anti-Stokes Raman spectroscopy: A signature of dissociative pump–dump–pump wave packet dynamics

J. Faeder,[a] Iddo Pinkas, G. Knopp, Yehiam Prior, and D. J. Tannor[b]
Department of Chemical Physics, Weizmann Insitute of Science, 76100 Rehovot, Israel

(Received 30 May 2001; accepted 27 August 2001)

Knopp *et al.* [J. Raman Spectrosc. **31**, 51 (2000)] have recently used resonant femtosecond coherent anti-Stokes Raman spectroscopy (CARS) to prepare and probe highly excited vibrational wave packets on the ground electronic potential surface of molecular iodine. The experiment uses a sequence of three resonant femtosecond pulses with two independently variable time delays. The first two pulses act as a pump and dump sequence to create a predefined, highly excited wave packet on the ground electronic state, whose amplitude is optimized by selecting the proper pump–dump (Raman) frequency difference and varying the time delay. The third pulse promotes the pump–dump wave packet to an excited electronic state, resulting in subsequent coherent emission of light at the anti-Stokes frequency. This fully-resonant CARS signal, measured as a function of time delay between the second and third pulses, oscillates at a frequency characteristic of the pump–dump wave packet. Due to anharmonicity, this frequency is a sensitive measure of the amount of vibrational excitation. Knopp *et al.* observed that under certain conditions the signal exhibits pronounced beating between the pump–dump wave packet frequency and the frequency characteristic of the bottom of the ground state well. In this paper we show that these beats arise only when the final pump–dump–pump wave packet is above the excited state dissociation threshold of the molecule. We derive analytical expressions showing that under these conditions, where the polarization is short-lived, there may be strong interferences between the contributions from molecules originally in different vibrational states of the thermal ensemble. In contrast, the CARS polarization in the below threshold case is long-lived, and these interferences cancel. Numerical evaluation of the CARS signal through vibrational wave packet propagation confirms the predictions of the analytical theory and reproduces the distinctive beating pattern observed in the experiments. Additional experiments and simulations demonstrate that these interferences can be turned on or off by carefully selecting the pulse frequencies. The experiments can also be viewed from a different perspective, as an extension of the pump–dump mechanism for selective bond breaking on the ground electronic state, to a pump–dump–pump sequence for selective bond breaking on the excited electronic state. © *2001 American Institute of Physics.*
[DOI: 10.1063/1.1412253]

I. INTRODUCTION

A series of recent experiments have successfully produced and probed highly vibrationally excited wave packets on the ground electronic state of diatomic molecules.[1–6] This ability to selectively pump large amounts of energy into a specific molecular motion represents an important first step towards control of chemical reaction dynamics. Vibrational excitation was produced by a sequence of two femtosecond pulses; a ''pump'' pulse creating a wave packet on an excited electronic state, followed by a ''dump'' pulse of longer wavelength that drops the wave packet back to the ground electronic state at higher vibrational energy than the initial state. These experiments realize a scheme first proposed for the control of ground state reaction dynamics more than 15 years ago.[7–9] The key step in the process is the introduction of a variable delay time between the pump and dump pulses, which allows the excited wave packet to reach regions of the excited state potential with favorable transition probabilities back to excited regions of the ground state potential.

In principle, many other parameters, such as the frequencies, bandwidths, and phases of the pulses can be used to further manipulate ground state wave packets.[7,10–15] For example, Shen *et al.* have recently shown that nearly complete population transfer is possible using shaped pump and dump pulses.[15] Nevertheless, an impressive degree of control of ground state wave packet preparation has already been achieved experimentally using only the time delay as the control parameter. Brown *et al.*[16] showed that selective excitation of a ground state wave packet could be achieved even with degenerate wavelength pump and dump pulses by varying only the time delay. Pausch *et al.* have produced highly excited ground state vibrational wave packets in a molecular beam of K_2 using the pump–dump scheme and probed them

[a]Current address: Theoretical Biology and Biophysics Group, MS K710, Los Alamos National Laboratory, Los Alamos, New Mexico 87545.
[b]Author to whom correspondence should be addressed. Electronic mail: David.Tannor@weizmann.ac.il

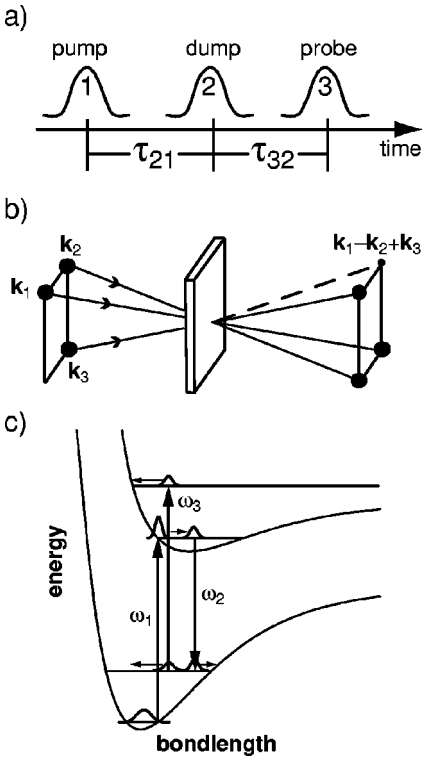

FIG. 1. Schematic illustration of femtosecond CARS with two time delays. (a) Laser pulses. (b) Incoming and outgoing laser beams. Incoming beams are labeled by their incident wave vectors, and the outgoing signal is emitted in the phase-matching direction $\mathbf{k}_1-\mathbf{k}_2+\mathbf{k}_3$. (c) Wave packet creation and evolution.

via multiphoton ionization.[1,2] Neumark and co-workers have used pump–dump to create and detect ground state wave packets as high as 98% of the dissociation threshold in gas phase I_2^- using femtosecond photoelectron spectroscopy.[3,4] Finally, Knopp, Pinkas, and Prior have generated and detected ground state wave packets in I_2 having up to half of the ground state dissociation energy, using two-dimensional time delay coherent anti-Stokes Raman spectroscopy $[(\mathrm{TD})^2\mathrm{CARS}]$.[5,6]

Whereas the above mentioned schemes use femtosecond pulses and generate the desired wave packet within a single vibrational period, there are also well-established techniques for the generation of highly excited vibrational states on time scales much longer than a vibrational period. Stimulated emission pumping (SEP),[17] which has been extensively used,[18,19] is the continuous wave version of the pump–dump scheme described above. The best that can be achieved with this technique, however, is total saturation of the population in all states involved. The more elaborate approach of stimulated Raman adiabatic passage (STIRAP),[20] based on adiabatic following, can transfer population efficiently between ground states without populating the intermediate excited state.

The $(\mathrm{TD})^2$CARS scheme is illustrated in Fig. 1. A ''pump'' pulse first creates a wave packet in an excited electronic state, and then a ''dump'' pulse of longer wavelength returns this wave packet to the ground electronic state. The wave packet created by the pump–dump sequence is optimized by timing the dump pulse to occur when the excited state wave packet enters the Franck–Condon region favorable for the dump transition,[5] as illustrated in Fig. 1(c). The third pulse re-excites this pump–dump wave packet, resulting in subsequent coherent emission of light in the phase-matched direction, $\mathbf{k}_1-\mathbf{k}_2+\mathbf{k}_3$ [see Fig. 1(b)],[21,22] centered around the anti-Stokes frequency, $\omega_{\mathrm{AS}}=\omega_1-\omega_2+\omega_3$. The CARS signal is measured as a function of the time delay between the dump and probe pulses ($\tau_{32}=\tau_3-\tau_2$), for a fixed time delay between the pump and dump (τ_{21}), providing a map of the ground state wave packet dynamics. In principle there are eight dynamical pathways that may contribute to the resonant four-wave mixing signal in the CARS direction;[23–26] however, as we describe in more detail in Sec. II B, the large detuning of the dump pulse effectively eliminates all but the pump–dump–probe sequence illustrated in Fig. 1.

Although time-resolved CARS has been widely used in condensed phases to measure vibrational dephasing and relaxation,[27–38] it has been applied to the gas phase only relatively recently.[5,6,39–46] Hayden and Chandler[39] performed femtosecond CARS experiments on gas phase benzene and 1,3,5-hexatriene and observed a decay of the signal on a 1–10 ps time scale. They attributed this decay to vibration-rotation interaction in the case of benzene and decay of spatial orientation in the case of hexatriene. Rubner *et al.*[43] have performed femtosecond CARS on gas phase benzene, toluene, and benzene/toluene mixtures and observed interference between the contributions from different molecules, an effect that had been observed much earlier in liquids.[30,31] In these experiments neither the pump nor the probe is resonant with an excited electronic state, and thus the CARS polarization exists only during the probe pulse. As we show in this paper, the lifetime of the induced polarization determines whether intermolecular interferences are observed.

Closely related to the present work are the experiments of Schmitt *et al.*,[40–42,44] who used femtosecond CARS to monitor the evolution of wave packets in the ground state of I_2. Apkarian and co-workers[38,45,46] have also used femtosecond CARS to monitor ground state dynamics of I_2 both in gas phase and rare gas matrices, and have used optical gating to time resolve the CARS polarization. In these experiments each of the pulse interactions is fully resonant between the ground X and excited B states of I_2. Meyer *et al.*[47–50] used perturbative wave packet calculations[51] and very recently nonperturbative calculations[52,53] to calculate the time-dependent CARS signal, obtaining good agreement with the experiments. There are two main differences between the fully resonant measurements on I_2 and the gas phase CARS transients from hydrocarbons involving nonresonant probing. First, the 200 cm^{-1} ground state vibrational frequency of I_2 is observed directly in the transients, because the pulse bandwidths are broad enough to excite several vibrational states simultaneously, producing a wave packet. Second, the CARS signal persists for probe delay times of tens to hundreds of picoseconds even though there is a broad distribution of initially populated vibrational and rotational states.

The $(\mathrm{TD})^2$CARS scheme of Knopp *et al.*[5,6] differs from the previous time domain experiments by the introduction of a time delay between the pump and dump pulses, which is

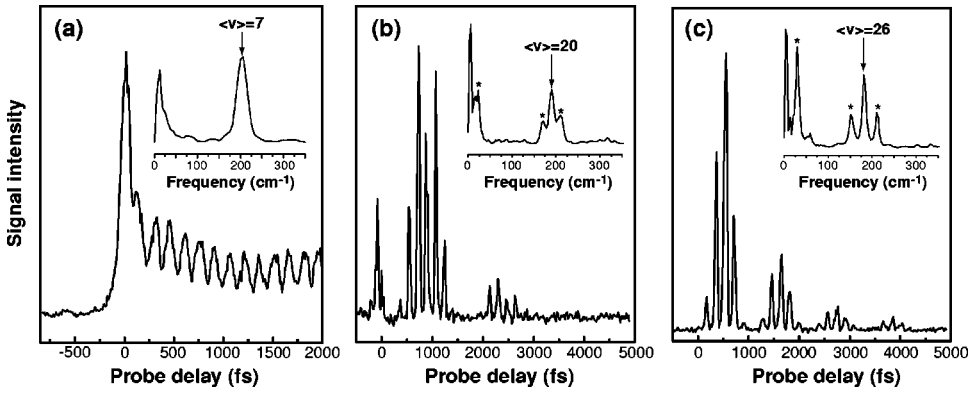

FIG. 2. $(TD)^2$CARS experiments with increasing levels of vibrational excitation. The pump/dump/probe frequencies and pump–dump (Raman) frequency differences are (a) 585/637/585 nm, $\omega_{12}=1400\,\mathrm{cm}^{-1}$; (b) 585/730/585 nm, $\omega_{12}=3400\,\mathrm{cm}^{-1}$; (c) 585/800/585 nm, $\omega_{12}=4600\,\mathrm{cm}^{-1}$.

used to optimize the signal from the ground state wave packet. A series[5] of $(TD)^2$CARS transients, for increasing levels of vibrational excitation, is shown in Fig. 2. The Fourier transforms, shown as insets, each display a peak indicated by arrows, at the characteristic frequency of the pump–dump wave packet. The figure also indicates the average vibrational quantum number in each case. As the vibrational excitation increases, the peak shifts to lower frequency due to anharmonicity in the X state potential well. In addition, the transients in (b) and (c) display strong low frequency beats, which show up at the frequencies marked by the asterisks, and decay to zero on a time scale of 5–10 ps. These features were previously noted and their frequencies properly assigned, but their origin was not understood.

In this paper we develop a theoretical description of the $(TD)^2$CARS transients based on both an analytical treatment as well as detailed numerical simulations using wave packets. We find that the beating is a manifestation of interference between the polarizations produced in separate molecules starting from different initial vibrational states; hence the description ''vibrational polarization beats.'' This term is meant to distinguish this effect from *quantum beats* that occur due to coherent evolution of the quantum wave function of a single molecule. We show that the appearance of polarization beats in the I_2 experiments correlates with the final probe excitation creating a wave packet above the dissociation threshold of the molecule, resulting in a very short polarization lifetime. In contrast, in the below threshold case, the polarization is long-lived, and the contributions from different initial vibrational states cancel.

The remainder of this paper is organized as follows: In Sec. II we present a brief review of the formalism of time-dependent four-wave mixing applied to CARS and then derive an analytical expression for the $(TD)^2$CARS signal in the eigenstate basis. We evaluate this expression in the two limiting cases that the final excited wave packet is either above or below the excited state dissociation threshold, finding interference terms in the above threshold case that account for the experimentally observed beating frequencies. Section III describes numerical evaluation of the $(TD)^2$CARS signal using perturbative wave packet propagation, and Sec. IV presents comparisons between the results of simulations and experiments. The numerical simulations do not include the rotational degrees of freedom; the effect of rotational motion will be the subject of a future investigation. The simulation results verify the qualitative picture of vibrational polarization beats derived analytically, and show that vibrational effects account for most of the features in the experimental signals. Finally, Sec. V presents concluding remarks.

II. THEORY

In this section we derive an expression for the resonant $(TD)^2$CARS signal using a wave function description and time-dependent perturbation theory. Time domain CARS has been described theoretically in condensed phases using both phenomenological[27,29,30,35,54] and full quantum mechanical descriptions with density matrices.[24,55–57] A wave function description has also been given[58] and applied recently to resonant time domain CARS on I_2 in the gas phase.[38,45–50] A complementary density matrix description has also recently been developed by Dantus and co-workers[59–61] to describe three-pulse degenerate four-wave mixing (DFWM) experiments on iodine vapor. Many excellent reviews of the theory of nonlinear optical spectroscopy are available in the literature.[23,24,62–64] We adopt a wave function description here because the CARS technique lends itself to simple interpretation in terms of the wave packets shown in Fig. 1(c). We start our theoretical description of the $(TD)^2$CARS with some basic definitions in Sec. II A. In Sec. II B we present a diagrammatic representation of resonant four-wave mixing using double-sided Feynman diagrams[23–26,65] to illustrate the connection between the wave function and density matrix pathways that contribute to the signal. In Sec. II C we derive an expression for the CARS signal in the eigenstate basis and evaluate it assuming either a discrete set of final energy levels with narrow linewidths or a continuum of final levels, the latter case corresponding to probing above the dissociation threshold in the excited state.

A. Preliminaries

As a starting point, we consider the Hamiltonian of a molecule with two electronic states, g and e, coupled to an electric field consisting of a sequence of laser pulses. The Hamiltonian is

$$\hat{H}=\hat{H}_{\mathrm{mol}}+\hat{H}_{\mathrm{int}} \tag{1}$$

with

$$\hat{H}_{\rm mol}=\sum_n |gn\rangle\langle gn|\hbar\omega_{gn}+\sum_m |em\rangle\langle em|\hbar\omega_{em}, \quad (2)$$

where n and m are indices of the adiabatic rovibrational eigenstates of electronic potential surfaces g and e, respectively. The pulses assume the form

$$E(t)=\sum_i E_i(t)=\epsilon_i(t-\tau_i)e^{-i\omega_i(t-\tau_i)+i\mathbf{k}_i\cdot\mathbf{x}}, \quad (3)$$

where each pulse is centered at time τ_i, has carrier frequency ω_i, is incident at wave vector $\mathbf{k}_i$, and has a time dependent envelope given by $\epsilon_i(t-\tau_i)$. Within the rotating wave approximation, the interaction of the molecule with the field is given by

$$\hat{H}_{\rm int}=-\hat{\mu}^+E(t)-\hat{\mu}^-E^*(t), \quad (4)$$

$$\hat{\mu}^+=\sum_{mn} |em\rangle\langle gn|\mu_{mn}, \quad (5)$$

$$\hat{\mu}^-=(\hat{\mu}^+)^\dagger=\sum_{mn} |gn\rangle\langle em|\mu_{nm}, \quad (6)$$

where $\hat{\mu}_{mn}$ and $\hat{\mu}_{nm}$ are matrix elements of the dipole moment operator, $\mu_{mn}=\langle em|\hat{\mu}|gn\rangle$. The dipole raising and lowering operators have been defined so that $\hat{\mu}^+E_i(t)$ promotes a ket in the ground state to the excited state, corresponding to absorption of light, and $\hat{\mu}^-E_i^*(t)$ demotes a ket in the excited state to the ground state, corresponding to stimulated emission.

B. Spectroscopic pathways

The fundamental observable in most forms of nonlinear spectroscopy, including CARS, is the third order polarization, $P^{(3)}$. First, we describe the terms that contribute to the polarization in a particular direction produced by a sequence of three pulses with different incident wave vectors, and then we discuss how a single dynamical pathway is selected by the $(\mathrm{TD})^2$CARS pulse sequence.

In order to calculate the third order polarization, we start with a perturbative expansion of the wave function,

$$|\psi(t)\rangle=|\psi^{(0)}(t)\rangle+|\psi^{(1)}(t)\rangle+|\psi^{(2)}(t)\rangle+|\psi^{(3)}(t)\rangle+\cdots, \quad (7)$$

where the wave function at each order is given iteratively as

$$|\psi^{(n)}(t)\rangle=(i\hbar)^{-1}\int_{-\infty}^{t}dt'e^{-i\hat{H}_{\rm mol}(t-t')/\hbar}\hat{H}_{\rm int}(t')|\psi^{(n-1)}(t')\rangle. \quad (8)$$

Through each succesive interaction with the field, the wave function acquires spatial dependencies associated with each of the pulses. So, for example, the first order wave function consists of the sum

$$|\psi^{(1)}(t)\rangle=|\psi^{(1)}_{\mathbf{k}_1}(t)\rangle+|\psi^{(1)}_{\mathbf{k}_2}(t)\rangle+|\psi^{(1)}_{\mathbf{k}_3}(t)\rangle. \quad (9)$$

The spatial dependence of each portion of the perturbative wave function thus identifies the sequence of interactions that it has undergone, marking a spectroscopic pathway. For higher order wave functions, the order of the wave vectors denotes the time order of interactions with the field, so that $|\psi^{(3)}_{\mathbf{k}_1-\mathbf{k}_2+\mathbf{k}_3}(t)\rangle$ is the wave function created by absorption of pulse 1, followed by stimulated emission of pulse 2, and finally absorption of pulse 3. The same sequence on the bra side gives the same wavevector dependence with the opposite sign.

We now examine the directionality of the third order polarization, which is the lowest order of polarization that can reflect the spatial dependence of all three incident pulses, and is the lowest order of polarization relevant to most forms of nonlinear spectroscopy. Neglecting molecular moments above dipole order, the polarization of an ensemble of molecules is simply the ensemble average of the molecular dipole moment. Thus we may define the molecular polarization, $P(t)\equiv\langle\psi(t)|\hat{\mu}|\psi(t)\rangle$. The third order contribution to the polarization is given by

$$P^{(3)}(t)=\langle\psi^{(0)}(t)|\hat{\mu}|\psi^{(3)}(t)\rangle+\langle\psi^{(2)}(t)|\hat{\mu}|\psi^{(1)}(t)\rangle+\text{c.c.} \quad (10)$$

The CARS signal is measured in the direction $\mathbf{k}_1-\mathbf{k}_2+\mathbf{k}_3$. In general, four terms may contribute to the third order polarization in this direction,

$$\begin{aligned}P^{(3)}_{\mathbf{k}_1-\mathbf{k}_2+\mathbf{k}_3}(t)=&\langle\psi^{(0)}(t)|\hat{\mu}|\psi^{(3)}_{\mathbf{k}_1-\mathbf{k}_2+\mathbf{k}_3}(t)\rangle\\&+\langle\psi^{(0)}(t)|\hat{\mu}|\psi^{(3)}_{\mathbf{k}_3-\mathbf{k}_2+\mathbf{k}_1}(t)\rangle\\&+\langle\psi^{(2)}_{\mathbf{k}_2-\mathbf{k}_3}(t)|\hat{\mu}|\psi^{(1)}_{\mathbf{k}_1}(t)\rangle\\&+\langle\psi^{(2)}_{\mathbf{k}_2-\mathbf{k}_1}(t)|\hat{\mu}|\psi^{(1)}_{\mathbf{k}_3}(t)\rangle+\text{c.c.}\end{aligned} \quad (11)$$

This expression includes all possible time orderings of the three interactions. The second and fourth terms are obtained from the first and third terms by interchanging the roles of pulses 1 and 3.

The spectroscopic pathways that produce the third order polarization in Eq. (11) may be depicted using double-sided Feynman diagrams,[23–26,65] as shown in Fig. 3. The four terms in Eq. (11) give rise to the eight diagrams, which describe all possible resonant paths for a system with two electronic states. Two equivalent interpretations of the diagrams are possible here. In terms of the wave function description we have used above, the diagrams represent the sequence of bra and ket interactions as a function of time, which runs from bottom to top. By convention, the ket path is shown on the left, and the bra path is shown on the right. Each interaction is represented by an arrow pointing towards the line to indicate absorption or away from the line to indicate emission. The wave vector dependence acquired from each interaction is also indicated. The second interpretation comes from the realization that the bra and ket considered together at a given time along the path constitute a portion of the density matrix, which describes the state of the system. When all of the system degrees of freedom are treated explicitly, the wave function and density matrix treatments produce the same observables, but the density matrix is more easily adapted to reduced dimensional treatments.[24]

The key difference between the wave function and density matrix formulations of $P^{(3)}$ lies in the time ordering of the interactions occuring on the bra and ket sides. The dia-

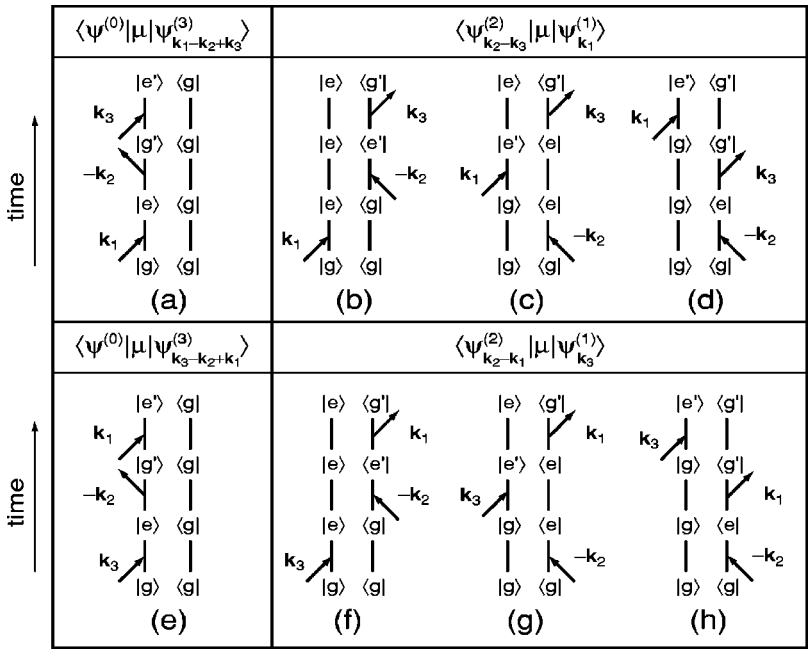

FIG. 3. The resonant double-sided Feynman diagrams for $P^{(3)}$ in the direction $\mathbf{k}_1-\mathbf{k}_2+\mathbf{k}_3$ and their correspondence with the wave function terms in Eq. (11). Only two electronic states are considered. The primes indicate different rovibrational levels within an electronic state.

grams shown in Fig. 3 are fully time ordered with respect to both the bra and the ket interactions, while the terms appearing in Eq. (11) do not specify a time ordering between the bra and the ket. This is the reason there are eight density matrix pathways (corresponding to eight double-sided Feynman diagrams), but only four wave function pathways. As shown in Fig. 3, the wave function terms involving one interaction on the ket side and two on the bra side encompass three density matrix pathways, with the ket interaction occurring before, between, or after the two bra interactions. The two wave function terms involving $|\psi^{(3)}(t)\rangle$, on the other hand, each correspond to only a single density matrix pathway.

The goal of $(TD)^2$CARS is to probe the dynamics of the ground state wave packet created by the pump–dump sequence, which corresponds to the signal created by pathway (a). A $(TD)^2$CARS transient is measured by scanning the second time delay, τ_{32}, for a fixed value of the pump–dump time delay, τ_{21}.[5] Thus, the signal reflects the dynamics of the system during the second evolution period of the diagrams in Fig. 3. Half of the pathways evolve on the ground state, e.g., pathway (a) in $|g'\rangle\langle g|$, while the other half evolve on the excited state, e.g., pathway (b) in $|e\rangle\langle e'|$. Even when none of the pulses overlap, in which case only pathways (a) and (b) survive, both ground and excited state dynamics contribute to the signal in the absence of an additional selective mechanism.

There are two primary mechanisms for the enhancement of ground state contributions to the $(TD)^2$CARS signal, both of which are most clearly understood in the frequency domain. Since the goal of $(TD)^2$CARS is to create highly excited vibrational wave packets on the ground state, we can assume that the frequency difference between the pump and dump pulses is large compared to the vibrational level spacing and kT, and furthermore that the pump and dump pulse bandwidths do not overlap. The first selective mechanism arises because all of the pathways involving the second order wave function, $\psi^{(2)}$, require absorption of the dump pulse from the initial state. If the pump excitation is near the center of the electronic absorption band, then the cross section for absorption of the dump pulse will be very small, perhaps zero if the frequency difference is large enough that excitation with the dump pulse is nonresonant. Furthermore, the effect of weak dump absorption is not effected by the pulse timing, since absorption always occurs from the initial state, which is assumed to be stationary. On the other hand, the pump–dump time delay is used to optimize stimulated emission by the dump pulse, selectively enhancing the signal from pathway (a). Setting a nonzero pump–dump time delay also eliminates any contribution from pathway (e), which involves interactions with the pump, dump, and probe in reverse order, and contributes only when all three pulses overlap.

The second mechanism for selectivity is complementary to the first. All of the pathways involving $\psi^{(2)}$ also require stimulated emission by either the pump or probe pulses following absorption by the dump pulse. As a result, the final state energy of the bra wave function is shifted from the initial state energy by $\hbar(\omega_3-\omega_2)$, as illustrated by the level diagram in Fig. 4(b). As long as $\hbar(\omega_3-\omega_2)\gg kT$, there is no population of initial states with energy high enough to undergo dump absorption and probe stimulated emission, thus eliminating the pathways involving $\psi^{(2)}$. Note that this second mechanism is independent of the first and may operate even when the dump absorption cross section is not negligible. Although in most CARS applications, $\omega_1=\omega_3$, the above condition for selection of ground state dynamics is less restrictive, and it may be useful, as we discuss later, to probe at frequencies lower than the pump.

C. The CARS signal

In this section we derive an expression for the third order polarization and CARS signal in the eigenstate representa-

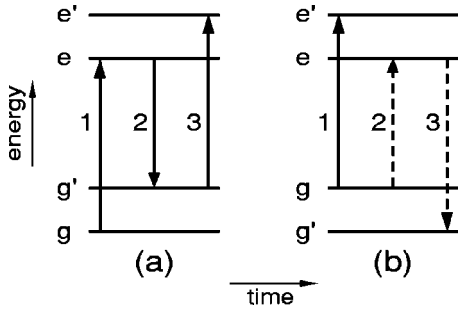

FIG. 4. Energy level diagrams for the first two pathways in Fig. 3. The solid arrows indicate the ket path, while the dashed arrows indicate the bra path. Diagrams for the remaining pathways are obtained by interchanging the labels 1 and 3, and for (b) by changing the position of the ket excitation to be between or after the two bra interactions.

tion. As discussed above, under typical experimental conditions for $(TD)^2$CARS experiments, only pathway (a) makes a significant contribution to the polarization. Thus, we write

$$P^{(3)}(t)\approx P^{\mathrm{CARS}}(t)\equiv\langle\psi^{(0)}(t)|\hat{\mu}|\psi^{(3)}_{\mathbf{k}_1-\mathbf{k}_2+\mathbf{k}_3}(t)\rangle+\mathrm{c.c.} \tag{12}$$

Applying the perturbation theory given by Eq. (8) to third order, and using the Hamiltonian in Sec. II A, we find

$$\begin{aligned}P^{\mathrm{CARS}}(t)=\frac{-i}{\hbar^3}\sum_{fjni}p_i\mu_{if}\int_{-\infty}^{t}dt_3\int_{-\infty}^{t_3}dt_2\int_{-\infty}^{t_2}dt_1e^{-i\omega_{fi}(t-t_3)}\\ \times[\mu_{fj}E_3(t_3)]e^{-i\omega_{ji}(t_3-t_2)}[\mu_{jn}E_2^*(t_2)]\\ \times e^{-i\omega_{ni}(t_2-t_1)}[\mu_{ni}E_1(t_1)]+\mathrm{c.c.},\end{aligned} \tag{13}$$

where each term in the sum represents an amplitude for creating polarization via the path $|gi\rangle\rightarrow|en\rangle\rightarrow|gj\rangle\rightarrow|ef\rangle$, as illustrated in Fig. 5. These paths are summed over the possible initial states weighted by the initial occupation probabilities, p_i, which are determined from a Boltzmann distribution. During each period between interactions, the amplitude acquires a phase due to the frequency difference between the currently occupied level and the initial level, given by $\omega_{fi}=\omega_{ef}-\omega_{gi}$, $\omega_{ji}=\omega_{gj}-\omega_{gi}$, etc. It is this phase that causes oscillation in the CARS signal as each of the delay times is varied. In order to make explicit how the amplitudes depend on the delay times between the pulse centers, $\tau_{21}=\tau_2-\tau_1$ and $\tau_{32}=\tau_3-\tau_2$, we substitute the pulse

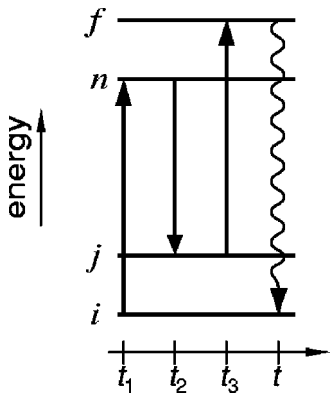

FIG. 5. Indices of the energy levels occupied along the CARS path.

definitions given in Eq. (3) into Eq. (13) and change integration variables to $T=t-\tau_3$; $T_i=t_i-\tau_i$, $i=1-3$, which yields

$$\begin{aligned}P^{\mathrm{CARS}}(T)=\frac{-i}{\hbar^3}\sum_{fjni}p_i\mu_{if}e^{-i\omega_{fi}T}e^{-i\omega_{ji}\tau_{32}}e^{-i\omega_{ni}\tau_{21}}\\ \times G_{fjni}(T)+\mathrm{c.c.},\end{aligned} \tag{14}$$

where

$$\begin{aligned}G_{fjni}(T)=\int_{-\infty}^{T}dT_3\,\mu_{fj}\epsilon_3(T_3)e^{-i(\omega_3-\omega_{fj})T_3}\\ \times\int_{-\infty}^{T_3+\tau_{32}}dT_2\,\mu_{jn}\epsilon_2^*(T_2)e^{i(\omega_2-\omega_{nj})T_2}\\ \times\int_{-\infty}^{T_2+\tau_{21}}dT_1\,\mu_{ni}\epsilon_1(T_1)e^{-i(\omega_1-\omega_{ni})T_1}.\end{aligned} \tag{15}$$

$G_{fjni}(T)$ is a convolution of partial Fourier transforms of the pulse envelopes at the difference between the carrier frequency of each pulse and the appropriate transition frequency along the path. The time delays between pulses and between the final pulse and detection enter only in the upper limits of the integrals, so that when these delay times are large, G becomes a product of individual Fourier transforms,

$$G_{fjni}(T\gg 0)\rightarrow\mu_{fj}\overline{\epsilon_3}(\omega_{fj})\mu_{jn}\overline{\epsilon_2^*}(\omega_{nj})\mu_{ni}\overline{\epsilon_1}(\omega_{ni}), \tag{16}$$

where

$$\overline{\epsilon_i}(\omega)=\int_{-\infty}^{\infty}dt\,\epsilon_i(t)e^{-i(\omega_i-\omega)t}. \tag{17}$$

Equation (16) becomes an excellent approximation for pulses separated by more than a few pulse widths. In the simulations described in Sec. III, the CARS signal is evaluated numerically, so the main purpose of expressing the polarization in this form is to demonstrate that the primary effect of scanning the delay time between pulses 2 and 3 is to add a phase $e^{i\omega_{ji}\tau_{32}}$ to each term in the polarization. The fact that this phase depends on the frequency *difference* ω_{ji}, rather than on the frequency ω_{gj} alone, gives rise to the additional frequencies observed in the interference signal, as we describe below.

We may now write the polarization in the simple form,

$$P^{\mathrm{CARS}}(T)=\frac{-i}{\hbar^3}\sum_{if}p_ia_{fi}(T)e^{-i\omega_{fi}T}+\mathrm{c.c.}, \tag{18}$$

where

$$a_{fi}(T)=\mu_{if}\sum_{jn}e^{-i\omega_{ji}\tau_{32}}e^{-i\omega_{ni}\tau_{21}}G_{fjni}(T) \tag{19}$$

is the amplitude for the set of paths beginning in state i and ending in state f. Measurement of these amplitudes, and in particular their dependence on τ_{32} is the primary objective of time-dependent CARS experiments.

The simplest method for detecting the CARS signal is to collect all of the light emitted in the CARS direction, $\mathbf{k}_1-\mathbf{k}_2+\mathbf{k}_3$. This signal is given by

$$S=\int_{-\infty}^{\infty} dT\,|P^{\mathrm{CARS}}(T)|^2$$
$$=\frac{2}{\hbar^6}\sum_{ii',ff'} p_i p_{i'}\int_{-\infty}^{\infty} dT\,a_{fi}(T)a^*_{f'i'}(T)e^{-i(\omega_{fi}-\omega_{f'i'})T}, \tag{20}$$

where in the second line we have neglected the terms with the rapidly oscillating integrand $e^{i(\omega_{fi}+\omega_{f'i'})T}$ (rotating wave approximation). The central feature of this expression is the product of the two polarization amplitudes, $a_{fi}(T)$ and $a_{f'i'}(T)$, which gives rise to interferences between paths with different initial and final levels. From Eq. (19) we have

$$a_{fi}(T)a^*_{f'i'}(T)=\sum_{nn',jj'} G_{fjni}(T)G^*_{f'j'n'i'}(T)$$
$$\times e^{-i(\omega_{nn'}-\omega_{ii'})\tau_{21}}e^{-i(\omega_{jj'}-\omega_{ii'})\tau_{32}}. \tag{21}$$

The complex exponentials in this expression are the primary source of variation in the CARS signal when either of the time delays between pulses is scanned. The oscillations of the CARS signal arise from the phase difference between two paths connecting initial and final states. During each propagation period, the accumulated phase depends on two frequency differences: the frequency difference between the levels occupied during that period on each of the two paths and the frequency difference between the initial levels. For example, when τ_{32} is scanned, the accumulated phase is $e^{-i(\omega_{jj'}-\omega_{ii'})\tau_{32}}$, where $\omega_{jj'}$ is a frequency difference in the pump–dump wave packet, and $\omega_{ii'}$ is a frequency difference between the initial levels. As discussed below, when the final states are discrete and well-separated, the $i\neq i'$ and $f\neq f'$ terms in the signal become negligible, leaving only contributions from frequency differences in the pump–dump wave packet. An example of the $(\mathrm{TD})^2$CARS signal with final states below the dissociation threshold is shown in Fig. 2(a), where the signal is plotted as a function of the dump-probe delay time, τ_{32}. The dominant frequency component, $204\,\mathrm{cm}^{-1}$, is the average energy spacing, $\omega_{jj'}$, in the pump–dump wave packet with an average vibrational quantum number $\langle v\rangle\approx 7$.

As also discussed below, contributions to the signal from interferences between pathways with different initial and final levels are observed when the final states lie in the continuum, i.e., are above the dissociation threshold of the excited state. Examples are shown in Figs. 2(b) and 2(c). For the 585/800/585 nm experiment [Fig. 2(c)], the average frequency difference in the pump–dump wave packet with an average vibrational quantum number $\langle v\rangle=26$ is about $180\,\mathrm{cm}^{-1}$, while the average frequency difference in the initial thermal ensemble is about $210\,\mathrm{cm}^{-1}$. According to Eq. (21), the lowest order interference terms occur for $i=i'+1$ and $j=j'$ at $210\,\mathrm{cm}^{-1}$, $i=i'+1$ and $j=j'+1$ at $30\,\mathrm{cm}^{-1}$, and $i=i'+1$ and $j=j'+2$ at $150\,\mathrm{cm}^{-1}$. These frequencies match very well with those found in the Fourier transform of the experimental transient.

The fact that interference contributions can arise between paths with different initial levels is perhaps surprising, since in a thermal ensemble there is no phase relationship between the initial states i and i'. These initial states are distinguishable in the quantum mechanical sense, and thus may not interfere directly. The interferences in the CARS signal, however, arise when the *polarizations* produced by two different pathways cannot be resolved in the frequency domain, i.e., when the difference ω_{fi} and $\omega_{f'i'}$ is much smaller than the lifetime of the observed polarization. This condition is embedded in Eq. (20) through the exponential term, $e^{-i(\omega_{fi}-\omega_{f'i'})T}$, that, in the absence of a decay mechanism for the $a_{fi}(T)$, imposes the resonance condition $\omega_{fi}=\omega_{f'i'}$. It is also illustrative to express the CARS signal in the frequency domain as

$$S=\sum_{ii'} p_i p_{i'}\int_{-\infty}^{\infty} d\omega P_i(\omega)P^*_{i'}(\omega). \tag{22}$$

The $i=i'$ terms in the sum are the integrated intensities of the polarizations arising from each initial level, and constitute an incoherent average over different initial states. The $i\neq i'$ terms come from the spectral overlap of polarizations from different initial states and are the interferences. When the spectra of the polarizations consist of a set of narrow, nonoverlapping lines, the interferences will be small, but when the spectra of the polarizations are continuous the overlap and give rise to large interferences.

The label ''polarization beats'' has been used previously to distinguish these types of interferences from those involving coherent evolution of the quantum wave function, ''quantum beats.'' [24,47,66–68] While quantum beats may originate within a single molecule, the polarization beats are entirely an intermolecular effect, since each molecule in a thermal ensemble may be considered to be in a single initial state. Although polarization beats are generally assumed to contain no dynamical information,[24] the magnitude of these interference terms is quite sensitive to how the system is probed; in particular, the density of final state energy levels. We now investigate two limiting cases that correspond well with experimental conditions: first, when the final states are discrete and well-separated and second, when the final states lie in a continuum.

1. Discrete set of final states

For all but the simplest potential and pulse shapes the CARS signal in Eq. (20) must be evaluated numerically because of the complex time dependence of the amplitudes $a_{fi}(T)$ during the probe pulse. After the probe pulse has ended, however, the amplitudes are effectively constant, and it is then straightforward to evaluate the long time contributions the the signal. Formally, we may define a cutoff time, T_c, which will typically be a few pulse widths, and divide the contibutions to the signal as

$$S_{\mathrm{total}}=S_<+S_> \tag{23}$$

with

$$S_<=\frac{2}{\hbar^6}\sum_{ii',ff'} p_i p_{i'}\int_{-\infty}^{T_c} dT\,a_{fi}(T)a^*_{f'i'}(T)e^{-i(\omega_{fi}-\omega_{f'i'})T}, \tag{24}$$

$$S_{>}=\frac{2}{\hbar^6}\sum_{ii',ff'} p_i p_{i'} a_{fi} a^{*}_{f'i'} \int_{T_c}^{\infty} dT\, e^{-i(\omega_{fi}-\omega_{f'i'})T}, \tag{25}$$

where $a_{fi}=\lim_{T\to\infty} a_{fi}(T)$. It is instructive to consider the possibility of interference contributions to $S_{<}$, even though we may see immediately that in the absence of dissipative processes the total signal will be dominated by δ function spikes in $S_{>}$ that occur when $\omega_{fi}=\omega_{f'i'}$. The products $a_{fi}(T)a^{*}_{f'i'}(T)$ are functions that vary on the time scale of the pulse width, and hence have a width in frequency space comparable to the bandwidth of the probe pulse. Thus, pairs of paths with frequency differences that are within the probe pulse bandwidth will contribute to the signal at short times, and vibrational polarization interferences would be observed if contributions from the short and long time signals could be separated.

In the gas phase the molecular polarization decays due to such processes as collisions, spontaneous emission, and dephasing of the molecular ensemble due to a distribution of velocities (Doppler broadening). These processes effectively introduce a linewidth in the polarization spectrum, which in principle, if large enough could allow interferences to occur. Pastirk *et al.*[69] have recently measured dephasing of vibronic coherences between the X and B states of molecular iodine in the gas phase, finding polarization lifetimes of about 200 ps over the temperatures 350–380 K, the range relevant to the $(TD)^2$CARS experiments. This lifetime includes both homogeneous and inhomogeneous decay mechanisms. Since this time scale is much longer than the approximately 100 fs time scale necessary to produce coherent vibrational excitation, it is reasonable to include the polarization decay only in $S_{>}$. If we assume the polarization decays exponentially as $e^{-\gamma T}$, then

$$S_{>}=\frac{2}{\hbar^6}\sum_{ii',ff'} p_i p_{i'} a_{fi} a^{*}_{f'i'} \left(\frac{e^{-i(\omega_{fi}-\omega_{f'i'})T_c}}{2\gamma+i(\omega_{fi}-\omega_{f'i'})}\right). \tag{26}$$

The frequency difference in the denominator causes interference terms to be small unless a substantial fraction of frequency differences $\omega_{fi}-\omega_{f'i'}$ contributing to the signal are small compared with γ. In other words, the interferences become an important contributor to the total signal only when there is substantial overlap in the spectra arising from different initial states. In the long lifetime limit, i.e., no spectral overlap, the signal becomes an incoherent sum over initial and final states, Eq. (26),

$$S_{\mathrm{long}}=\frac{1}{\gamma\hbar^6}\sum_{if} p_i^2 |a_{fi}|^2. \tag{27}$$

From Eqs. (26) and (27) it is clear that the long time contribution to the signal is inversely proportional to γ, and hence is much larger than the short time signal for typical gas phase dephasing times.

A numerical example of the CARS signal for probe excitation to a set of discrete final levels is shown in Fig. 6. Part (a) shows the short time signal, $S_{<}$, and its decomposition into $i=i'$ contributions and $i\neq i'$ contributions. The former, labeled S_{ii}, represents an incoherent averaging over contributions to the polarization from different initial vibrational states, and its Fourier transform contains only the frequencies of the vibrational level spacing in the pump–dump wave packet. The dominant component is due to the first difference, $\omega_j-\omega_{j-1}$. Narrowing of the modulation depth results from the distribution of level spacings in the wave packet. The interference contributions, labeled $S_{i\neq i'}$ are comparable in magnitude to S_{ii} and produce a strong low frequency modulation of the total signal. The Fourier transform of $S_{i\neq i'}$ displays three primary peaks attributable to different combinations of level spacings in the initial state distribution and the pump–dump wave packet. The primary beat frequency is approximately the difference between the average energy level spacing of initial states and the average spacing in the pump–dump wave packet. Part (b) of Fig. 6 shows the total CARS signal for $S_{>}$ evaulated using two

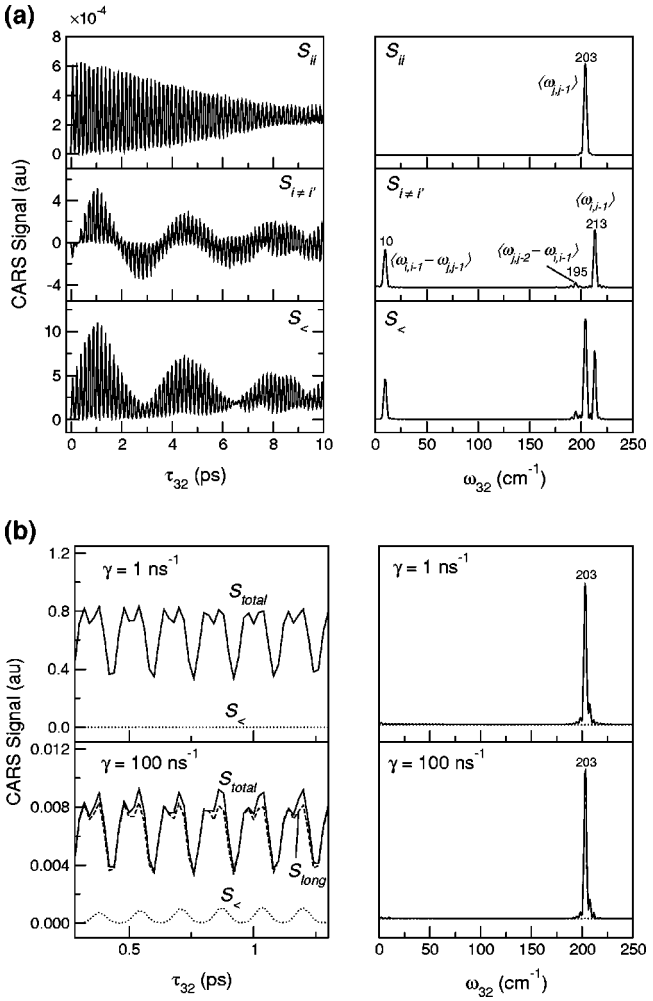

FIG. 6. $(TD)^2$CARS signal for probe excitation to a discrete set of final levels. (a) Short-time signal, $S_{<}$, divided into contributions from paths with the same initial vibrational level, S_{ii}, and paths with different initial vibrational levels, $S_{i\neq i'}$. (b) Total signal, $S_{\mathrm{total}}=S_{<}+S_{>}$, with $S_{>}$ computed using two different exponential decay constants, γ. The long lifetime limit of the signal, S_{long} [see Eq. (27)], is shown with dashed lines, but is indistinguishable from S_{total} in the $\gamma=1\ \mathrm{ns}^{-1}$ case. Note the difference in the scale of the signal between (a) and (b); the contributions from $S_{>}$ mask the interferences in $S_{>}$. The small auxiliary peaks in the Fourier transforms of S_{long} arise from resolution of the different energy level spacings in the pump–dump wave packet, not polarization interferences. The simulation parameters are for 551/604/551 nm excitation of I_2 with 50 fs FWHM Gaussian pulses at 360 K. See Sec. III and top panel of Fig. 10 for details.

different values of the decay rate γ. For a decay rate typical of gas phase experiments, $\gamma = 1\ \mathrm{ns}^{-1}$, the contribution of $S_<$ to the total signal is negligible, and $S_<$ makes only a very modest contribution even for a very fast decay rate. In addition, interference effects in the long time signal are too small to observe in both cases, and S_{long} [see Eq. (27)] is an excellent approximation to the total signal. Thus, when the probe excitation is to a discrete and well-separated set of final levels, the CARS signal is accurately described as an incoherent average over signals arising from different initial and final states. Finally, it should be noted that the double-peaked structure in the oscillations of the transients in Fig. 6(b) is not observed in the oscillations of $S_<$. Karavitis *et al.* have shown that this period doubling arises from passage of the pump–dump wave packet passing through the probe window region twice during each oscillation period.[38] The component arising from passage through the region with positive momentum is effectively filtered in the $S_<$ because the final state wave packet with positive momentum does not return to the Franck–Condon region for anti-Stokes emission until after the cutoff time.

2. Continuum set of final states

Probe excitation to the continuum above the molecular dissociation threshold unmasks the polarization interferences in the short-time signal. Physically, dissociation of the molecule insures that the long-time polarization is zero, since the polarization is the transition moment weighted overlap of the wave packet created by the probe with the initial state wave function [see Eq. (12)]. Formally, taking the continuum limit of Eq. (18), we may write

$$P^{\mathrm{CARS}}(T) = \frac{-i}{\hbar^3} \sum_i p_i e^{i\omega_i T} \int_{-\infty}^{\infty} d\omega_f a_i(\omega_f, T) e^{-i\omega_f T} + \mathrm{c.c.}, \tag{28}$$

where $a_i(\omega_f, T)$ is the amplitude associated with going from state i to a final state in the continuum at energy $\hbar\omega_f$. The CARS polarization in Eq. (28) appears as the inverse Fourier transform of the transition amplitude distribution, $a_i(\omega_f, T)$, whose bandwidth is determined by a convolution of the excitation pulse bandwidths. Hence, the polarization decays to zero after at most a few pulse widths and we can pick T_c so that $S_>$ is zero. Now, as before, the change in $a_i(\omega_f, T)$ during the pulse effectively couples paths with different initial and final states, leading to polarization interferences in the total signal, and these are no longer masked by a signal from after the pulse.

The square magnitude of the CARS polarization as a function of T and τ_{32} is displayed for both a discrete and a continuum example in Fig. 7. The polarization in (a), where the final energy is below the dissociation threshold, continues at large T values; whereas the polarization in (b), above the dissociation threshold, remains at zero after about 100 fs. The pulses are Gaussian with a 50 fs full width half maximum.

Simulations of the particularly dramatic beats that arise in the $(\mathrm{TD})^2$CARS experiments at high vibrational excitations are displayed in Fig. 8. The S_{ii} contribution to the signal show an average vibrational spacing of about

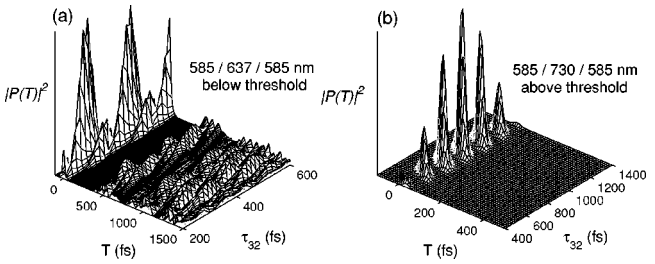

FIG. 7. Square magnitude of the $(\mathrm{TD})^2$CARS polarization as a function of the dump-probe time delay, τ_{32}, and the time after the center of the third pulse, T. Contributions from all initial levels are added coherently. The simulation parameters are the same as in (a) and (b) of Fig. 9. In (a), final states are below dissociation threshold, while in (b) they are above the threshold.

$180\ \mathrm{cm}^{-1}$, but is otherwise very similar to the S_{ii} transient shown in Fig. 6 for the discrete level case. The large $S_{i\neq i'}$ contributions also produce a strong beating in the total short time signal and give rise to the additional peaks in the Fourier transform spectrum with the assignments shown. The transients from the discrete level and continuum case examples are remarkably similar, but the key difference is that $S_>$ vanishes in the continuum case, allowing the interferences to be observed. The disappearance of the long time contribution to the signal means that the total CARS intensity in the continuum case will be several orders of magnitude smaller than in the discrete level case, as the simulations demonstrate. The zero-background detection of the four-wave mixing signal, however, permits detection of the much weaker signal. In principle, it would also be possible to measure the short time signal, even for discrete level probing, by time gating the CARS polarization in order to recover the polarization interferences.

III. SIMULATION METHODS

Propagation of the time-dependent wave functions on a coordinate grid is a practical way of evaluating the

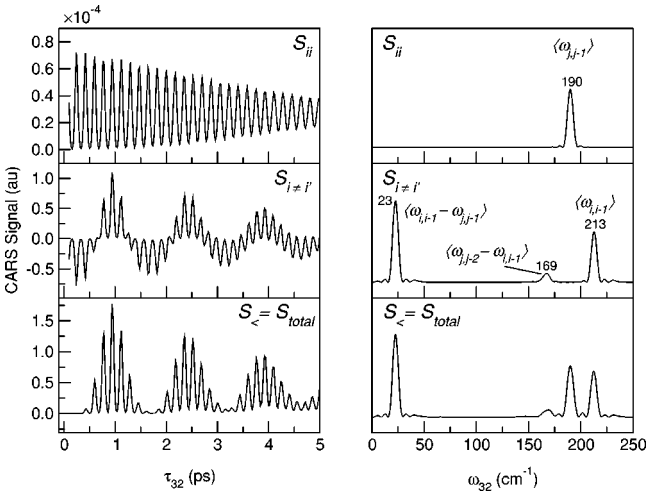

FIG. 8. $(\mathrm{TD})^2$CARS signal for probe excitation to a continuum set of final levels. The simulation parameters are for 585/730/585 nm excitation of I_2 at 360 K, which produces a large change in the ground state level spacing. See Sec. III and Fig. 9 for details.

$(TD)^2$CARS signal numerically. Engel has developed a simple scheme for evaluating perturbative wave functions iteratively[51] and has recently applied this to calculate femtosecond CARS and DFWM signals.[47–50,53] We follow essentially the same method, but as discussed below, it is necessary to avoid some additional approximations made by those workers in order to obtain the polarization beats in the CARS signal. We now briefly describe the wave packet calculations and the relevant parameters used to obtain the results.

The nth order wave function is propagated forward in time using

$$|\psi^{(n)}(t+\Delta t)\rangle = e^{-i\hat{H}\Delta t/\hbar}|\psi^{(n)}(t)\rangle - \frac{i}{\hbar}\Delta t\hat{V}(t+\Delta t)|\psi^{(n-1)}(t+\Delta t)\rangle, \quad (29)$$

where $\hat{V}$ is the perturbation and $|\psi^{(n-1)}\rangle$ is the wave function at order $n-1$. For calculation of nonlinear spectroscopy, each spectroscopic path, consisting of a sequence of interactions with different field components, is computed as a separate wave function. For each wave function containing n interactions with the field that contributes to the desired signal, there is a cost of n wave packet propagations, although there is some redundancy among the different terms that contribute to the signal. In order to calculate all four terms in Eq. (11) that contribute to the third order polarization in the CARS direction, a total of nine wave packet propagations must be performed. In all of the simulations reported here, we have computed all four terms in the third order polarization in order to check that the CARS term [pathway (a) in Fig. 3] dominates the signal. For all of the experimental conditions we have simulated in this work, we have found nearly complete selectivity for this pathway.

For the simulations of the above threshold probe, the third order polarization is obtained numerically and integrated to obtain the signal. The polarization decays rapidly to zero after the probe pulse, and therefore a propagation of $|\psi^{(3)}(t)\rangle$ for only a few pulse widths is sufficient. In simulations of the below threshold probe, it is impractical and unnecessary to extend the wave packet propagation over the duration of the polarization signal, which is infinite in the absence of damping (nonzero γ). As long as the CARS pathway dominates the signal, the incoherent sum in Eq. (27) is the most accurate and practical approach. The necessary components $|a_{fi}|^2$ are obtained simply by projecting the third order wave function onto the eigenfunction basis at a time after the third pulse has effectively ended, to compute

$$|a_{fi}|^2 = |\mu_{fi}|^2|c_f|^2, \quad (30)$$

where c_f is the coefficient of the eigenfunction f in the final state wave function, $|\psi^{(3)}(t)\rangle$. In previous simulations, the below threshold CARS signal was computed as an incoherent sum over initial states with the polarization integrated for a few hundred femtoseconds, essentially one oscillation period of the final state wave packet.[47–50,53] In our simulations we have found that this method results in a significant phase shift of the CARS signal as a function of τ_{32} when τ_{21} is nonzero.

The single surface wave packet propagations, which correspond to the first term on the right hand side of Eq. (29), are performed using the split operator method[70] using fast Fourier transforms to switch between position and momentum representations. A 256 point grid with a minimum and maximum of 2.28 and 5.82 Å and a stepsize in time of 0.1 fs provide converged results for all of the calculations we report here. The potential curves for the X and B state of I_2 were the same as those used by Jonas *et al.*,[71] who used a high order interpolation scheme based on earlier RKR potentials.[72,73] The standard Morse potentials used in simulations of I_2 dynamics give inaccurate level spacings for the high vibrational states accessed in the experiments. The pulse envelopes in Eq. (3) are taken to be Gaussians of the form,

$$\epsilon_i(t) = \epsilon_0 e^{-(t-t_i)^2/2\sigma^2}, \quad (31)$$

where $\sigma = \mathrm{FWHM}/(2\sqrt{\ln 2})$ when FWHM is the full width at half maximum of the pulse *intensity*. In all of the simulations, FWHM is set to 50 fs. The X to B state electronic transition dipole moment was taken to be a constant function of bond length. The product $\mu\epsilon_0$ was set to 7×10^{-4} atomic units, but is unimportant to the results, since only relative intensities are reported. The remaining parameters, τ_{21} and the pulse carrier frequencies, are reported in the figures showing the simulation results.

We have neglected the rotational degree of freedom in these calculations. At the experimental temperatures, hundreds of intial rotational states are thermally populated, making their inclusion in the simulation cumbersome. Rotational degrees of freedom have been taken into account at varying levels of approximation in previous simulations of time domain CARS transients.[39,43,47,49,50] Two primary effects have been attributed to rotational degrees of freedom in time domain CARS and four-wave mixing in general.[74–76] First, there is a short-time transient due to rotational anisotropy that decays rapidly during the first 1–2 ps and is essentially flat out to the rotational recurrence time, which may extend to hundreds of picoseconds.[75,76] This effect has been observed in both resonantly[5,6,40,42,44] and nonresonantly[39,43] probed time domain CARS in the gas phase and may be eliminated, at least for the case of coincident pump and dump pulses, by using the magic angle polarization geometry.[44] Second, there is a longer time modulation or decay of the signal due to vibration-rotation interactions,[76] which causes the nonresonantly probed CARS signal to decay on a time scale of 5–10 ps.[39,43] This effect is also apparently observed in the $(TD)^2$CARS transients in cases where there is large vibrational excitation and the probing is above the dissociation threshold [see Figs. 2(b) and 2(c)], but is not seen in the below threshold transients[5,6,40,42,44] [Fig. 2(a)], which suggests that polarization interference effects play some additional role in the overall decay.

IV. COMPARISONS WITH EXPERIMENT

The comparison between the simulated and experimental results is shown in Fig. 9. Figure 9(a) shows the $(TD)^2$CARS transient for excitation at 581/631/581 nm; for this set of

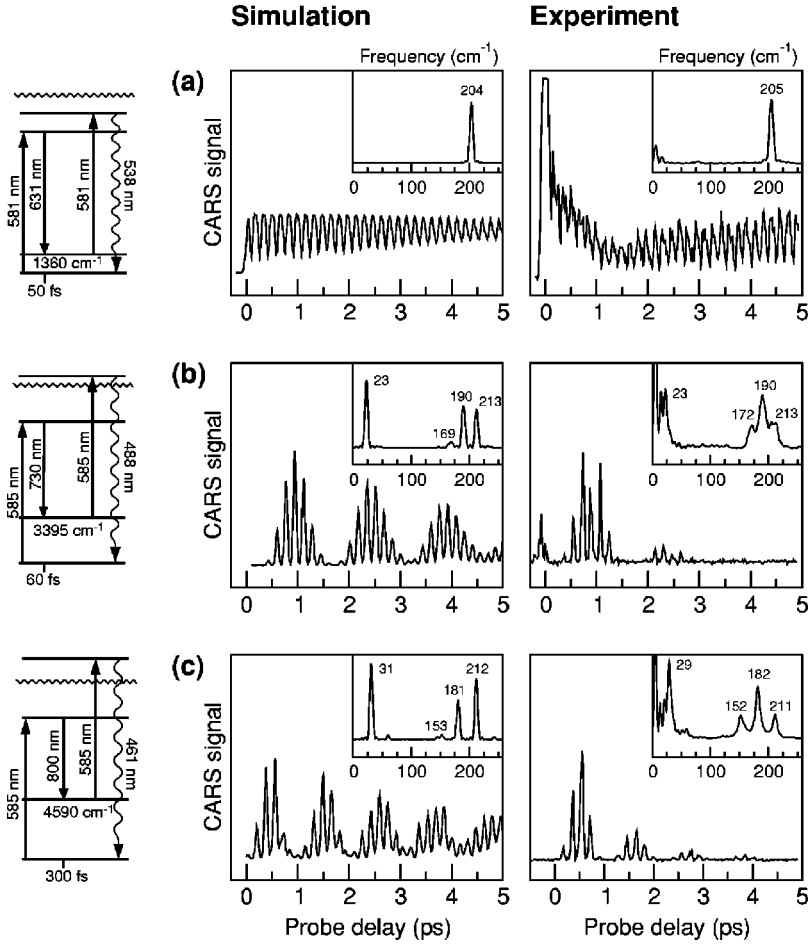

FIG. 9. Simulated and experimental (TD)^{2}CARS transients and their Fourier transforms (inset) for I_2 at 360 K. Pulse frequencies in (a) correspond to probing below the *B* state dissociation threshold (wavy line), while those in (b) and (c) correspond to probing above threshold. The labels in the inset graphs give the peak positions in wave numbers.

excitation frequencies the final states accessed by the probe pulse lie well below the threshold for dissociation in the *B* state. In this case the CARS polarization persists on a timescale that is very long compared to the pulse duration, and, as a result, there is no interference modulation of the signal. The basic periodicity of the signal corresponds to the average frequency difference between the vibrational levels populated in the pump–dump wave packet, $\langle \omega_{j,j-1} \rangle$. For the 581/631 nm pump and dump, the average vibrational quantum number is about 8, and the corresponding frequency difference is 204 cm^{-1}, which is the peak frequency present in the Fourier transform of the simulated transient. The frequency peak in the experimental spectrum is at 205 cm^{-1}. The experimental signal shows a large peak at zero time, followed by a decay over the first picosecond due to rotational anisotropy. This decay shows up at low frequencies of between 6 and 12 cm^{-1} in the Fourier transform spectrum, but is absent from the simulated transient, presumably due to the neglect of rotations. The simulated and experimental transients both display oscillations at the primary vibrational frequency, maintaining a fairly constant average signal intensity after the first picosecond. There is additional modulation of the simulated transient is due to anharmonicity and the excitation of more than two vibrational levels in the pump–dump wave packet. The additional modulation of the experimental signal differs from that of the simulation, possibly because of vibration-rotation interactions and differences between idealized pulse shapes in the simulations and the actual pulses in the experiments.

Figures 9(b) and 9(c) show the (TD)^{2}CARS transient for excitation at 585/730/585 nm and 585/800/585 nm, respectively. In contrast to Fig. 9(a), the pulse frequencies in Figs. 9(b) and 9(c) correspond to probing above the dissociation threshold for I_2 in the *B* state. Prominent beats now appear in the transients at frequencies of about 20 cm^{-1} in (b) and 30 cm^{-1} in (c). These beats shift to higher frequency as the amount of vibrational excitation is increased, and display complete modulation of the signal, i.e., the amplitude decays to near zero between the beats. The simulations accurately capture the beating and the distinctive structures of the transients, and there is excellent agreement in the positions of the transient oscillations for the full duration of the experimental signal (4–5 ps). The beats are particularly strong in Fig. 9(b) and 9(c) because the two initial vibrational levels, $v=1$ and 2, contribute almost equally to the signal. Both the simulated and experimental transients decay between successive beats, but the experimental decay is much faster, possibly due to a combination of vibration-rotation interactions and interference among the polarizations arising from different initial rotational levels.

The Fourier transforms of the (TD)^{2}CARS transients are shown in the insets of Fig. 9. Discrete peaks are observed at

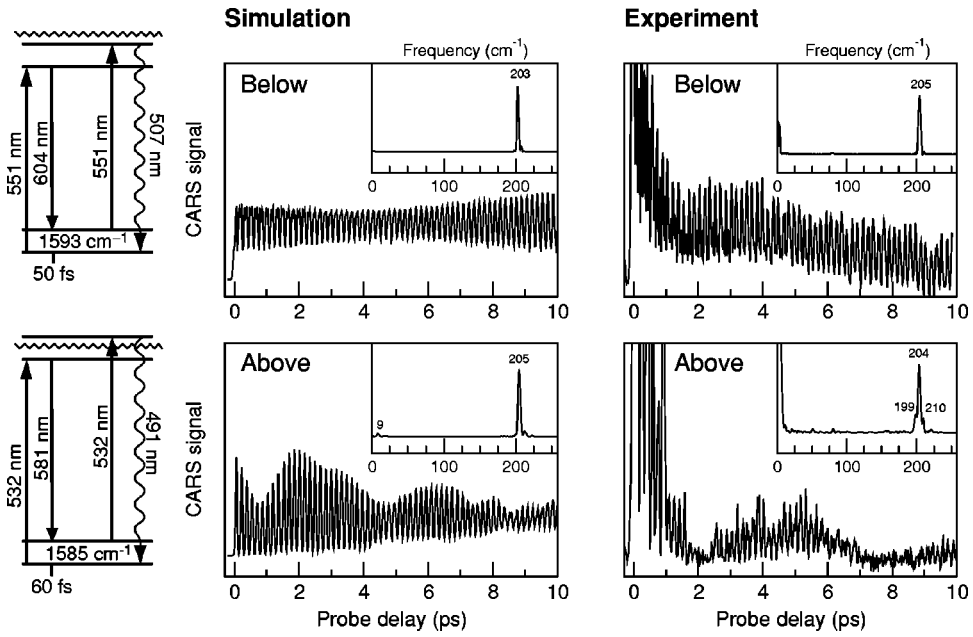

FIG. 10. Simulated and observed signals for below and above threshold probing of a ground state wave packet with approximately the same vibrational excitation.

the frequencies predicted by Eq. (21). There is a peak at the primary difference frequency, $\langle \omega_{j,j-1} \rangle$, which is 190 and 181 cm^{-1} for (b) and (c), respectively. The highest frequency peak occurs at about 212 cm^{-1} in both cases, and is just the average vibrational spacing in the initial ensemble, $\langle \omega_{i,i-1} \rangle$. The primary frequency responsible for the beating occurs at the difference of these two frequencies, $\langle \omega_{i,i-1} - \omega_{j,j-1} \rangle$, which is 23 cm^{-1} in (b) and 30 cm^{-1} in (c). Small peaks also occur at $\langle \omega_{j,j-2} - \omega_{i,i-1} \rangle$, which corresponds to about 170 and 150 cm^{-1} in (b) and (c), respectively.

To test our interpretation of the vibrational polarization beats, additional experiments and simulations were performed where the amount of vibrational excitation in the ground state was held fixed, while the energy of the probe wave packet was set to be either below or above the dissociation threshold. Figure 10 shows the experimental and simulated transients. Further details about the experimental setup can be found in Refs. 5 and 6. Theory predicts that there should be no vibrational interferences in the transients from below threshold probing, and no beating is observed in either the simulations or experiment. The simulated transient is very similar to the one shown in Fig. 9(a), except that the primary frequency is shifted slightly lower (about 203 cm^{-1}) because of the slightly higher vibrational excitation. The experimental transient is also similar to the one shown in Fig. 9(a), except that there is a larger contribution from the second harmonic of the primary frequency at early times, and a significant decay of the signal between about 5 and 10 ps. Only one significant peak near the primary vibrational frequency of 205cm^{-1} is observed. Theory predicts that vibrational interferences should occur in the transients with above threshold probing, and indeed significant beating is observed in both the simulations and the experiments (lower panels of Fig. 10). According to the theory, the frequency of the vibrational beating should be $\langle \omega_{i,i-1} - \omega_{j,j-1} \rangle$, which is about $7-9$ cm^{-1}, corresponding to a period of between 3.5 and 4.5 ps. In the experiment the peak corresponding to $\langle \omega_{i,i-1} \rangle$ occurs at 210 cm^{-1} and the period of the beats corresponds to about 5.5 cm^{-1}. The triplet structure of the Fourier transformed experimental transient (lower right) near the primary frequency is quite similar to those observed in Figs. 9(b) and 9(c). By comparison, the amount of interference in the simulated transient (lower left) is much smaller, resulting in a nonuniform modulation of the primary oscillation. A small peak near 9 cm^{-1} is found in the Fourier transform, but there is only a faint hint of the triplet structure in the spectrum near the primary frequency. The reason the vibrational interferences are small in the simulation is that the polarization from the initial vibrational level $v=0$ dominates the signal. Further simulations of the fully including rotational effects are needed account for the differences between the simulated and experimental transients.

Figure 11 displays experimental and simulated transients for pulse frequencies of 525/800/525 nm. Note that although the probe pulse is above the dissociation threshold, the beats have effectively disappeared. In fact, the experimental transient in Fig. 11 looks remarkably similar to the below threshold probe transients in Figs. 9 and 10. The disappearance of the beats is now a consequence of the *pump* frequency: at pump wavelengths shorter than about 530 nm, the amplitude for the initial excitation to the B state is dominated by $v=0$, effectively eliminating the interference contributions from other vibrational states. The Stokes shift of 6550 cm^{-1} is the largest obtained using $(\mathrm{TD})^2$CARS so far, creating a vibrational wave packet about 50% of the way up to the dissociation limit. There is reasonably good agreement between the simulated and observed signals after the decay of the rotational anisotropy. The decay in the amplitude of oscillation in the simulation is due to the large anharmonicity of the ground state potential at such a high excitation energy. It is also notable that the experimental transient does not decay appreciably after the first picosecond, in sharp contrast to the other experimental above-threshold transients with

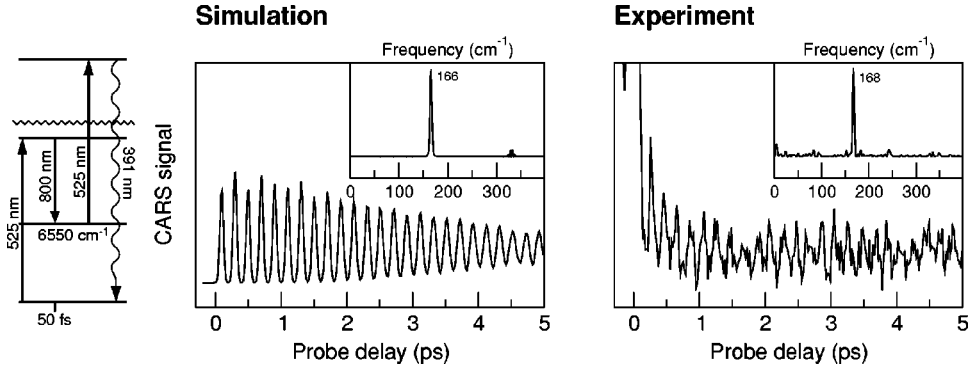

FIG. 11. Elimination of polarization beats by tuning pump and probe to higher frequencies. The pump–dump wave packet has $\langle v \rangle \approx 34$.

large vibrational excitation shown in Figs. 9(b) and 9(c). While the 525 nm pump excition selectively excites a single vibrational level, many rotational levels are still excited, and one might expect polarization interferences arising from different initial rotational states to cause a decay of the signal. Once again, additional simulations including rotation will be needed to determine to account fully for the observed signals.

The suppression of the polarization beats described in the previous paragraph does not continue as the pump and probe are further increased, because the probe excitation becomes nonresonant as the final probe states move to higher energies above the dissociation threshold. Already for 515/800/515 nm excitation, the CARS pathway becomes too weak to observe, and the experimental signal is dominated by a pathway involving excitation to the *B* state and lower lying *A* state, respectively, by the first two pulses.[6] Perhaps a more robust, way to suppress the beats would be to use a lower probe frequency to keep the final excitation below the dissociation threshold, or, alternatively, to tune the probe to a frequency in resonance with a third electronic state. Both of these possibilities are experimentally challenging, however, and we leave them for future investigation.

V. CONCLUSIONS

In this paper we have shown that vibrational polarization beats may arise in $(TD)^2$CARS when the excited wave packet produced by the pump–dump sequence is probed above the *B* state dissociation threshold. In previous time domain CARS experiments on I_2,[40,42,44,45] the wave packet was probed resonantly, with the final states lying below the the *B* state dissociation threshold, and hence no vibrational polarization beats were observed. In the experiments of Knopp *et al.*,[5,6] when the energy of the pump–dump excitation was increased, the probe step created a wave packet above the dissociation threshold, leading to a very short polarization lifetime and strong vibrational polarization beats.

Our theoretical description of the vibrational polarization beats indicates that this effect arises exclusively from intermolecular effects, i.e., interferences between polarizations on different molecules. These interferences between the polarizations on different molecules average to zero when the polarization lifetimes are long enough to resolve the individual contributions arising from different initial and final states,[47] e.g., for probing in the discrete region of the spectrum. Interference effects become large, however, when the polarization lifetime is short, such as when the molecule is probed above the excited state dissociation threshold. Numerical simulations verify this theoretical description and demonstrate that vibrational polarization beating accounts nearly quantitatively for the unusual transients that were observed in the experiments. We have also shown that a requirement for the beats is the thermal population of more than one initial vibrational states, and that the beats may be eliminated through selective excitation of a single initial vibrational state. A more general approach to eliminate the beats might be to lower the probe frequency so that the final excitation remains below the excited state dissociation threshold. The analytical theory, as well as the simulations, show that the CARS polarization persists for the entire radiative lifetime or dephasing time of the excited state, which in the gas phase is approximately a nanosecond. This long polarization has recently been observed experimentally in the elegant experiments of Zadoyan and Apkarian,[45,46] who time-resolved the CARS polarization produced in I_2 using the same pulse frequencies as Schmitt *et al.*[42] and observed rotational coherences up to 100 ps after the probe excitation.

Resonantly probed gas phase CARS thus offers the possibility of tuning the polarization lifetime and the resulting interference effects by adjusting the frequency of the probe excitation. Since the polarization lifetime in inherently short in nonresonantly probed four-wave mixing, intermolecular polarization interferences will always occur. In resonant condensed phase four-wave mixing the polarization lifetime is limited by the electronic dephasing time. Polarization interferences involving different initial vibrational states may thus provide a sensitive measure of the electronic dephasing time in condensed phases.

The utility of intermolecular, or macroscopic, interference in nonlinear spectroscopy and potentially optimal control of chemical reactions has recently been emphasized by Lozovoy *et al.*,[61] who used phase matching conditions to separate the microscopic and macroscopic contributions to the signal in various FWM experiments on I_2 vapor. They have suggested that modulation of the sample polarization though macroscopic effects (polarization interferences) may act as an important ''control knob'' in addition to microscopic interferences. Whether polarization interferences, such as those discussed here, can be exploited as a mecha-

nism for controlling chemical reactions is an important, and as yet unanswered, question.

While the present study has emphasized the usefulness of $(TD)^2$CARS as an effective spectroscopic tool, the same experiments may be viewed from a different perspective, as active control of chemical bond breaking. The first two steps in the $(TD)^2$CARS pulse sequence, with their variable time delay, correspond exactly to the pump–dump approach to active control of chemical bond breaking.[7–10,13–15] Early exploration of the pump–dump scheme indicated, that although control of bonding breaking via pump–dump is possible in principle, some variations on the scheme would be required to make it viable for most molecules.[8,77,78] The reason is that the scheme exploits energy picked up by the wave packet on the excited electronic state to break bonds in the ground electronic state. Since excited state bond strengths are normally significantly weaker than those in the ground state, it is not generally possible to pick up enough energy in the excited state to break a ground state bond. If, however, the role of ground and excited states were to be reversed, i.e., if one could somehow pump to the ground electronic state, preparing a highly excited vibrational wave packet on the ground state, and then ''dump'' to the excited state, one would be in a position to use the large ground state energies accumulated by the wave packet to break the weaker excited state bonds.[79] A convenient way to achieve this reversal of the ground and excited states is by a three pulse, pump–dump–pump sequence, in which the wave packet is first pumped to the excited state, dumped back to the ground state, and finally repumped to the excited state.[78] This pump–dump–pump sequence is precisely the $(TD)^2$CARS experiment introduced by Knopp *et al.*[5,6] and analyzed here. The potential for active control is obscured in I_2, since there is only one bond, but we believe that this potential should become apparent in future studies on polyatomic molecules. In principle, $(TD)^2$ CARS may be capable of producing controllable excited state dissociation in polyatomics, at the same time that it produces a robust, background-free, directional signal.

ACKNOWLEDGMENTS

One of the authors (J.F.) would like to thank Dr. Sarah Gallagher Faeder for many illuminating discussions about nonlinear spectroscopy and help in preparing the figures. Professor Ilya Averbukh is acknowledged for helpful comments and Dr. Peter Stern for help with computing resources. The work was supported in part by a grant from the Minerva Foundation and from Mrs. Rita Marcus, New York and also by the Israel Science Foundation (Mokad 8009/98 and 128/0).

[1] P. Pausch, M. Heid, T. Chen, W. Kiefer, and H. Schwoerer, J. Chem. Phys. **110**, 9560 (1999).
[2] R. Pausch, M. Heid, T. Chen, H. Schwoerer, and W. Kiefer, J. Raman Spectrosc. **31**, 7 (2000).
[3] M. T. Zanni, A. V. Davis, C. Frischkorn, M. Elhanine, and D. M. Neumark, J. Chem. Phys. **112**, 8847 (2000).
[4] A. V. Davis, M. T. Zanni, C. Frischkorn, M. Elhanine, and D. M. Neumark, J. Electron Spectrosc. Relat. Phenom. **112**, 221 (2000).
[5] G. Knopp, I. Pinkas, and Y. Prior, J. Raman Spectrosc. **31**, 51 (2000).
[6] I. Pinkas, G. Knopp, and Y. Prior, J. Chem. Phys. **115**, 236 (2001).
[7] D. J. Tannor and S. A. Rice, J. Chem. Phys. **83**, 5013 (1985).
[8] D. J. Tannor, R. Kosloff, and S. A. Rice, J. Chem. Phys. **85**, 5805 (1986).
[9] D. J. Tannor and S. A. Rice, Adv. Chem. Phys. **70**, 441 (1988).
[10] S. A. Rice and M. Zhao, *Optical Control of Molecular Dynamics* (Wiley, New York, 2000).
[11] E. M. Hiller and J. A. Cina, J. Chem. Phys. **105**, 3419 (1996).
[12] G. Ashkenazi, U. Banin, A. Bartana, R. Kosloff, and S. Ruhman, Adv. Chem. Phys. **100**, 229 (1997).
[13] Y. J. Yan, J. W. Che, and J. L. Krause, Chem. Phys. **217**, 297 (1997).
[14] Y. J. Yan, Z. W. Shen, and Y. Zhao, Chem. Phys. **233**, 191 (1998).
[15] Z. Shen, Y. Yan, J. Cheng, F. Shuang, Y. Zhao, and G. He, J. Chem. Phys. **110**, 7192 (1999).
[16] E. J. Brown, I. Pastirk, B. I. Grimberg, V. V. Lozovoy, and M. Dantus, J. Chem. Phys. **111**, 3779 (1999).
[17] C. E. Hamilton, J. L. Kinsey, and R. W. Field, Annu. Rev. Phys. Chem. **37**, 493 (1986).
[18] *Molecular Dynamics and Spectroscopy by Stimulated Emission Pumping*, vol. 4 in *Advanced Series in Physical Chemistry*, edited by H.-L. Dai and R. W. Field (World Scientific, Singapore, 1995).
[19] M. Drabbels and A. M. Wodtke, J. Phys. Chem. A **103**, 7142 (1999).
[20] K. Bergmann, H. Theuer, and B. W. Shore, Rev. Mod. Phys. **70**, 1003 (1998).
[21] Y. Prior, Appl. Opt. **19**, 1741 (1980).
[22] J. A. Shirley, R. J. Hall, and A. C. Eckbreth, Opt. Lett. **5**, 380 (1980).
[23] Y. R. Shen, *The Principles of Nonlinear Optics* (Wiley, New York, 1984).
[24] S. Mukamel, *The Principles of Nonlinear Optical Spectroscopy* (Oxford University Press, New York, 1995).
[25] T. Joo, Y. Jia, J.-Y. Yu, M. J. Lang, and G. R. Fleming, J. Chem. Phys. **104**, 6089 (1996).
[26] E. J. Brown, Q. Zhang, and M. Dantus, J. Chem. Phys. **110**, 5772 (1999).
[27] A. Laubereau and W. Kaiser, Rev. Mod. Phys. **50**, 607 (1978).
[28] B. H. Hesp and D. A. Wiersma, Chem. Phys. Lett. **75**, 423 (1980).
[29] D. D. Dlott, Annu. Rev. Phys. Chem. **7**, 157 (1986).
[30] R. Leonhardt, W. Holzapfel, W. Zinth, and W. Kaiser, Chem. Phys. Lett. **133**, 373 (1987).
[31] W. Zinth, R. Leonhardt, W. Holzapfel, and W. Kaiser, IEEE J. Quantum Electron. **24**, 455 (1988).
[32] H. Okamoto and K. Yoshihara, J. Opt. Soc. Am. B **7**, 1702 (1990).
[33] R. Inaba, H. Okamoto, K. Yoshihara, and M. Tasumi, J. Phys. Chem. **97**, 7815 (1993).
[34] M. Fickenscher, H. G. Purucker, and A. Laubereau, Chem. Phys. Lett. **191**, 182 (1992).
[35] T. Joo and A. C. Albrecht, J. Chem. Phys. **99**, 3244 (1993).
[36] T. Chen, A. Vierheilig, P. Waltner, M. Heid, W. Kiefer, and A. Materny, Chem. Phys. Lett. **325**, 176 (2000).
[37] T. Chen, A. Vierheilig, P. Waltner, M. Heid, W. Kiefer, and A. Materny, Chem. Phys. Lett. **326**, 375 (2000).
[38] M. Karavitis, R. Zadoyan, and V. A. Apkarian, J. Chem. Phys. **114**, 4131 (2001).
[39] C. C. Hayden and D. W. Chandler, J. Chem. Phys. **103**, 10465 (1995).
[40] M. Schmitt, G. Knopp, A. Materny, and W. Kiefer, Chem. Phys. Lett. **270**, 9 (1997).
[41] M. Schmitt, G. Knopp, A. Materny, and W. Kiefer, Chem. Phys. Lett. **280**, 339 (1997).
[42] M. Schmitt, G. Knopp, A. Materny, and W. Kiefer, J. Phys. Chem. A **102**, 4059 (1998).
[43] O. Rubner, M. Schmitt, G. Knopp, A. Materny, W. Kiefer, and V. Engel, J. Phys. Chem. A **102**, 9734 (1998).
[44] T. Siebert, M. Schmitt, A. Vierheilig, G. Flachenecker, V. Engel, A. Materny, and W. Kiefer, J. Raman Spectrosc. **31**, 25 (2000).
[45] R. Zadoyan and V. A. Apkarian, Chem. Phys. Lett. **326**, 1 (2000).
[46] R. Zadoyan, D. Kohen, D. A. Lidar, and V. A. Apkarian, Chem. Phys. (in press).
[47] S. Meyer, M. Schmitt, A. Materny, W. Kiefer, and V. Engel, Chem. Phys. Lett. **281**, 332 (1997).
[48] S. Meyer, M. Schmitt, A. Materny, W. Kiefer, and V. Engel, Chem. Phys. Lett. **287**, 753 (1998).
[49] S. Meyer, M. Schmitt, A. Materny, W. Kiefer, and V. Engel, Chem. Phys. Lett. **301**, 248 (1999).
[50] S. Meyer and V. Engel, J. Raman Spectrosc. **31**, 33 (2000).
[51] V. Engel, Comput. Phys. Commun. **63**, 228 (1991).
[52] L. Seidner, G. Stock, and W. Domcke, J. Chem. Phys. **103**, 3998 (1995).
[53] S. Meyer and V. Engel, Appl. Phys. B: Lasers Opt. **71**, 293 (2000).
[54] R. Leonhardt, W. Holzapfel, W. Zinth, and W. Kaiser, Rev. Phys. Appl. **22**, 1735 (1987).

[55] M. Hayashi, M. Sugawara, and Y. Fujimura, Phys. Rev. A **43**, 2416 (1991).
[56] M. Hayashi, Y. Fujimura, H. Okamoto, and K. Yoshihara, Chem. Phys. Lett. **196**, 44 (1992).
[57] V. F. Kamelov and Y. P. Svirko, Chem. Phys. Lett. **194**, 13 (1992).
[58] D. J. Tannor, S. A. Rice, and P. M. Weber, J. Chem. Phys. **83**, 6158 (1985).
[59] I. Pastirk, V. V. Lozovoy, B. I. Grimberg, E. J. Brown, and M. Dantus, J. Phys. Chem. A **103**, 10226 (1999).
[60] I. Pastirk, E. J. Brown, B. I. Grimberg, V. V. V. Lozovoy, and M. Dantus, Faraday Discuss. **113**, 401 (1999).
[61] V. V. Lozovoy, B. I. Grimberg, I. Pastirk, and M. Dantus, Chem. Phys. **267**, 99 (2001).
[62] W. T. Pollard and R. A. Mathies, Annu. Rev. Phys. Chem. **43**, 497 (1992).
[63] W. Domcke and G. Stock, Adv. Chem. Phys. **100**, 1 (1997).
[64] D. J. Tannor, "Interaction of light with matter: A coherent perspective," in *Encyclopedia of Chemical Physics and Physical Chemistry*, edited by J. H. Moore and N. D. Spencer (IOP, Philadelphia, 2000).
[65] S. Y. Yee, T. K. Gustafson, S. A. J. Druet, and J. P. E. Taran, Opt. Commun. **23**, 1 (1977).
[66] L. Q. Lambert, A. Compaan, and I. D. Abella, Phys. Rev. A **4**, 2022 (1971).
[67] M. Koch, J. Feldmann, G. von Plessen, E. O. Gbel, P. Thomas, and K. Köhler, Phys. Rev. Lett. **69**, 3631 (1992).
[68] J. Erland and I. Balslev, Phys. Rev. A **48**, R1765 (1993).
[69] I. Pastirk, V. V. Lozovoy, and M. Dantos, Chem. Phys. Lett. **333**, 76 (2001).
[70] M. D. Feit, J. A. Fleck, Jr., and A. Steiger, J. Comput. Phys. **47**, 412 (1982).
[71] D. M. Jonas, S. E. Bradforth, S. A. Passino, and G. R. Fleming, J. Phys. Chem. **99**, 2594 (1995).
[72] R. J. LeRoy, J. Chem. Phys. **52**, 2683 (1970).
[73] R. F. Barrow and K. K. Yee, J. Chem. Soc., Faraday Trans. 2 **69**, 684 (1973).
[74] A. B. Myers and R. M. Hochstrasser, J. Chem. Phys. **85**, 6301 (1986).
[75] P. M. Felker and A. H. Zewail, J. Chem. Phys. **86**, 2460 (1987).
[76] M. Gruebele and A. H. Zewail, J. Chem. Phys. **98**, 883 (1993).
[77] J. Somloi, V. A. Kazakov, and D. J. Tannor, Chem. Phys. **172**, 85 (1993).
[78] J. Somloi and D. J. Tannor, J. Phys. Chem. **99**, 2552 (1995).
[79] B. Amstrup, R. J. Carlson, A. Matro, and S. A. Rice, J. Phys. Chem. **95**, 8019 (1991).